# NapGH components of the periplasmic nitrate reductase of *Escherichia coli* K-12: location, topology and physiological roles in quinol oxidation and redox balancing

T. Harma C. BRONDIJK*, Arjaree NILAVONGSE*, Nina FILENKO*, David J. RICHARDSON† and Jeffrey A. COLE*[1]

*School of Biosciences, University of Birmingham, Birmingham B15 2TT, U.K., and †School of Biological Sciences, University of East Anglia, Norwich NR4 7TJ, U.K.

Nap (periplasmic nitrate reductase) operons of many bacteria include four common, essential components, *napD*, *napA*, *napB* and *napC* (or a homologue of *napC*). In *Escherichia coli* there are three additional genes, *napF*, *napG* and *napH*, none of which are essential for Nap activity. We now show that deletion of either *napG* or *napH* almost abolished Nap-dependent nitrate reduction by strains defective in naphthoquinone synthesis. The residual rate of nitrate reduction (approx. 1 % of that of $napG^{+}H^{+}$ strains) is sufficient to replace fumarate reduction in a redox-balancing role during growth by glucose fermentation. Western blotting combined with $\beta$-galactosidase and alkaline phosphatase fusion experiments established that NapH is an integral membrane protein with four transmembrane helices. Both the N- and C-termini as well as the two non-haem iron–sulphur centres are located in the cytoplasm. An N-terminal twin arginine motif was shown to be essential for NapG function, consistent with the expectation that NapG is secreted into the periplasm by the twin arginine translocation pathway. A bacterial two-hybrid system was used to show that NapH interacts, presumably on the cytoplasmic side of, or within, the membrane, with NapC. As expected for a periplasmic protein, no NapG interactions with NapC or NapH were detected in the cytoplasm. An *in vitro* quinol dehydrogenase assay was developed to show that both NapG and NapH are essential for rapid electron transfer from menadiol to the terminal NapAB complex. These new *in vivo* and *in vitro* results establish that NapG and NapH form a quinol dehydrogenase that couples electron transfer from the high midpoint redox potential ubiquinone–ubiquinol couple via NapC and NapB to NapA.

Key words: integral membrane protein, iron–sulphur protein, periplasmic nitrate reductase (Nap), quinol oxidation, topology, twin arginine targeting.

## INTRODUCTION

When *Escherichia coli* is grown in the absence of oxygen, nitrate is the preferred electron acceptor for anaerobic respiration. The *E. coli* genome encodes three distinct nitrate reductases. The membrane-bound nitrate reductases A and Z reduce nitrate in the cytoplasm [1–4]. Nitrate reductase A is the predominant nitrate reductase when *E. coli* is grown under nitrate-sufficient conditions [5], whereas nitrate reductase Z is poorly expressed under all growth conditions [3,6]. Under nitrate-limiting conditions, a Nap (periplasmic nitrate reductase) is expressed.

Naps have been found in many different organisms, where they fulfil different physiological roles depending on the species. They can function as electron sinks, e.g. during photosynthesis in *Rhodobacter sphaeroides* [7–9]; they are used for redox balancing during aerobic respiration on highly reduced carbon sources, e.g. during growth of *Paracoccus* with butyrate as the main source of carbon and energy [10]; and they may be used during anaerobic respiration, as in *E. coli* [11]. In spite of their different roles, there are several similarities between the Naps of different species. With few exceptions, they all share four proteins: NapA, NapB, NapC (or a homologue) and NapD. NapA and NapB form a complex in the periplasm, with the site of nitrate reduction on the NapA subunit and NapB functioning as an electron donor to NapA. NapC is located in the cytoplasmic membrane and is believed to be the quinol dehydrogenase of the complex [1]. NapD is located in the cytoplasm [1] and plays a role in NapA maturation [1,3].

In addition to these four common proteins, all Nap operons characterized so far encode between one and three additional proteins, usually of unknown function. In *E. coli*, Nap is encoded by the *napFDAGHBC* operon. On the basis of their primary structure, NapF, NapG and NapH are all predicted to be non-haem iron–sulphur proteins [12]. The cellular localization of these three proteins has not been determined, but it is believed that NapG is a periplasmic protein, NapH is an inner-membrane protein and NapF is thought to be in the cytoplasm, although its N-terminal sequence includes two arginine residues in a motif with some similarity to a TAT (twin-arginine targeting) export signal [14,15]. We have previously reported that mutants defective in the synthesis of nitrate reductase A, nitrate reductase Z and menaquinone grow slowly on the non-fermentable carbon source, glycerol, when nitrate is available as a terminal electron acceptor [16]. However, unlike the menaquinone-proficient parental strain, electron transfer from the quinol pool to nitrate is strongly dependent on NapG and NapH as well as on NapC. We have now determined the subcellular location of NapG and NapH and we provide a model for the secondary structure of NapH. Direct evidence that NapG and NapH are involved in ubiquinol oxidation, and also evidence for an unexpected role for the *E. coli* Nap in redox balancing, is also presented.

## MATERIALS AND METHODS

### Strains and growth conditions

Strains used in the present study are listed in Table 1. *E. coli* strains were grown aerobically in Luria–Bertani (LB) medium (10 g/l tryptone, 5 g/l yeast-extract and 5 g/l NaCl) or anaerobically in

Abbreviations used: LB, Luria–Bertani; $MKH_2$, reduced menaquinone; Nap, periplasmic nitrate reductase; TAT, twin-arginine targeting; $UQH_2$, reduced ubiquinone; X-Gal, 5-bromo-4-chloroindol-3-yl $\beta$-D-galactopyranoside; X-P, bromo-4-chloroindolyl phosphate.

[1] To whom correspondence should be addressed (e-mail j.a.cole@bham.ac.uk).

**Table 1** ***Escherichia coli*** **strains used in the present study**

| Strain | Relevant genotype | Source |
|---|---|---|
| BTH101 | F⁻ *cya-99 araD139 galE15 galK16 rpsL1* (Str$^r$) *hsdR2 mcrA1 mcrB1* | D. Ladant* [30] |
| JCB4041 | RK4353 Δ*narU-Z*::Ω Δ*narG-I* Δ*narL*::Tn10 | [16] |
| JCB4043 | JCB4041 Δ*napGH* | [16] |
| JCB4081 | JCB4041 Δ*nrfAB* Δ*nirBCD*::km | This work |
| JCB4083 | JCB4043 Δ*nrfAB* Δ*nirBCD*::km | This work |
| JCB4141 | JCB4041 Δ*menBC* | [16] |
| JCB4143 | JCB4043 Δ*menBC* | [16] |
| JCB4145 | JCB4041 Δ*menBC*Δ*napC* | [16] |
| RK4353 | Δ*lacU169 araD139 rpsL gyrA non* | [31] |
| TOP10 | F⁻ *mcrA* Δ*(mrr-hsd RMS-mcrBC)* Φ *80lacZ*Δ*M15* Δ*lacX74 deoR recA1 araD139* Δ*(araA-leu)697 galU galK* | Invitrogen |

* Institute Pasteur, Paris, France.

MS medium (4.5 g/l $KH_2PO_4$, 10.5 g/l $K_2HPO_4$, 1 g/l $NH_4SO_4$, 0.05 g/l $MgCl_2$, 2.5 g/l nutrient broth, 10 $\mu$M sodium molybdate, 10 $\mu$M sodium selenate and 1 ml/l of *E. coli* sulphur-free salts), supplemented with 20 mM $NaNO_3$ and 0.4 % (v/v) glycerol or 0.4 % (w/v) D-glucose. When appropriate, 100 $\mu$g/ml ampicillin and/or 50 $\mu$g/ml kanamycin were added. Unless stated otherwise, all cultures were grown at 37 °C.

### Construction of vectors for the overexpression of NapGH

Primers used are listed in Table 2. Plasmid pAN302N was constructed by amplifying a DNA fragment containing *napGH* using primers napGNcoI, which created an *Nco*I restriction site around the start codon of *napG*, and napHHindIII-2, which inserted an *Hin*dIII restriction site at the end of *napH* and omits the *napH* stop codon. As the *napG* coding region contains an *Nco*I restriction site, the *Nco*I fragment was first cloned into pBAD/*Myc*-His (Invitrogen), creating pAN301. The PCR fragment was then restricted with *Cla*I and *Hin*dIII and this fragment was cloned into pAN301, creating pAN302N. Plasmid pAN302 expresses untagged NapG and NapH–myc–$His_6$. To create plasmid pAN303, *napG* was amplified using primers napGNcoI and napGNdeImyc. The latter primer creates a myc tag at the C-terminus of *napG* and an *Nde*I restriction site after the stop codon. The *napH* coding region was amplified using primers napHNdeI and napHHindIII. The two fragments were then ligated into pBAD/myc-His. Primer napHHindIII includes the stop codon of *napH* and therefore plasmid pAN303 expresses NapG–myc and untagged NapH.

### Mutagenesis of *napG*

The twin-arginine motif in the putative signal sequence of NapG was changed into a double alanine using the Quickchange Site-Directed Mutagenesis kit (Stratagene) with primers napG(RR-AA)UP and napG(RR-AA)Down (Table 2) and plasmid pAN303 as the template. The final construct was called pAN306.

### Localization of myc-tagged proteins and Western-blotting procedures

Cultures were grown anaerobically in 1 litre of MS-glycerol/nitrate medium supplemented with 10 % (v/v) Lennox broth to an absorbance ($A_{650}$) 0.5 and induced with 0.02 % L-arabinose for 6 h. Bacteria were harvested, washed with 50 mM Tris/HCl (pH 8.0) and resuspended in 15 ml of 0.5 M sucrose, 5 mM EDTA and 50 mM Tris/HCl (pH 8.0). Lysozyme was added to give a final concentration of 600 $\mu$g/ml of bacterial suspension and the suspension was incubated for 1 h at 30 °C to release the periplasmic proteins. The sphaeroplasts were pelleted by centrifugation for 1 h at 12000 ***g***. The periplasmic fraction was dialysed against 1 mM Tris/HCl (pH 8.0), freeze-dried and resuspended in distilled water. The sphaeroplasts were resuspended in 5 ml of 5 mM $MgSO_4$/50 mM Tris/HCl (pH 8.0) and passed through a French pressure cell at 70 MPa. Unbroken bacteria and debris were removed by centrifugation at 5000 ***g*** for 5 min and the cytoplasmic and membrane fractions were separated by centrifugation at 170000 ***g*** for 1 h. The membrane fraction was further purified on a 36–54 % (w/v) sucrose gradient. Proteins were separated by SDS/PAGE and transferred to PVDF membrane. Anti-myc antibody was purchased from Invitrogen (Paisley, Scotland, U.K.) and anti-mouse IgG was obtained from TROPIX (Bedford, MA, U.S.A). The antibodies were detected using a chemiluminescence detection system (TROPIX).

### Construction of plasmids and detection of PhoA and LacZ fusion proteins

The *nap* operon, including its promoter, up to the desired fusion point in *napG* or *napH* was amplified using PCR. The primers introduced a *Pst*I or *Eco*RI site upstream of the *nap* promoter and a *Bam*HI site at the fusion point (Table 2). The *Pst*I–*Bam*HI fragments were cloned into pSK4158 [17] to create in-frame *phoA* fusions, and the *Eco*RI–*Bam*HI fragments into pNM480 [18] to create in-frame *lacZ* fusions. Transformants were plated on to selective LB agar with 40 $\mu$g/ml X-P (bromo-4-chloroindolyl

**Table 2 Primers used during this study**

| Name | Sequence 5′ → 3′ |
|---|---|
| napGNcoI | TTAACCATGGCCCGGTCAGCGAAACCTC |
| napGNdeImyc | TATTATCATATGCTATTACAGATCCTCTTCTGAGATGAGTTTTTGTTCCGATTTGCCATTGTTCCC |
| napG(RR-AA)up | CAAAATGGTGCCGCCCGCTTTCTGCGC |
| napG(RR-AA)down | CAGAAAGCGGGCACCATTTTGAGG |
| napHL27 | AATAGGATCCAACACCAGCCAACGGTGACTGCG |
| napHL58 | AATAGGATCCAACAGGCTACTGCTGTAGTTGCC |
| napHK101 | AATAGGATCCTTTCCCGCCAGGGCGTAGAGCACGG |
| napHS164 | AATAGGATCCGAAACGGGGTTGATCCATTCCC |
| napHstop | AATAGGATCCGATTTCGCTCCCGAACTCCATC |
| napHNdeI | TATTATCATATGGCAAATCGTAAACGTGACGCCGGG |
| napHHindIII | TATTATAAGCTTTCATGATTTCGCTCCCGAACTCC |
| napHHindIII-2 | TATTATAAGCTTTGATTTCGCTCCCGAACTCC |
| pnapFEcoRI | GAACGAATTCCCGATGATGTCGCTG |
| pnapFPstI | TATACTGCAGCCGATGATGTCGCTGAAGG |

phosphate) or 40 $\mu$g/ml X-Gal (5-bromo-4-chloroindol-3-yl $\beta$-D-galactopyranoside). PhoA and $\beta$-galactosidase activities were measured as described previously [19,20].

### Bacterial two-hybrid system

The gene of interest (*napC*, *napG* or *napH)* was cloned, with or without its stop codon, in-frame into pUT18, pUT18C or pKT25. The plasmids produce fusion proteins with the T18 and T25 fragments of *Bordella pertussis* adenylate cyclase [21]. Two complementary plasmids were transformed into *E. coli* BTH101. Transformants were plated on MacConkey agar supplemented with 1 % maltose plus 0.5 mM isopropyl $\beta$-D-galactopyranoside and incubated at 30 °C. Development of red colonies, indicative of a positive interaction, was followed for 72 h. The strength of the interactions was determined by measuring the $\beta$-galactosidase activity of the transformants after anaerobic growth to an $A_{650}$ of 0.5 in LB supplemented with 20 mM sodium nitrate and 0.4 % glycerol.

### Determination of quinol-nitrate oxidoreductase activities *in vitro*

A preculture of the appropriate *E. coli* strain was diluted 20-fold into LB supplemented with 20 mM sodium nitrate and 0.4 % glucose and grown anaerobically at 37 °C for 3–3.5 h. Cells were harvested and washed with 50 mM potassium phosphate (pH 7.0). Bacteria were resuspended in potassium phosphate buffer to an $D_{650}$ of approx. 40 and stored on ice. When required, the bacterial suspension was diluted to an $D_{650}$ of 2.0 in $N_2$-saturated potassium phosphate buffer and incubated at room temperature (approx. 22 °C). Quinones were dissolved to 50 mM in methanol and reduced by diluting 2-fold with 0.5 % $NaBH_4$ in 50 % (v/v) methanol. After a 5 min incubation, the residual $NaBH_4$ was degraded by the addition of 0.1 vol. of 0.1 M HCl. The reaction was started by the addition of 2.5 mM sodium nitrate and 1 mM reduced quinol to the cell suspension. Samples were removed at intervals, and the quantity of nitrite produced was determined [22].

### Rates of nitrate reduction by physiological substrates and reduced Methyl Viologen

A nitrate electrode was used to measure rates of nitrate reduction by washed bacterial suspensions incubated with 1.2 mM nitrate and the physiological substrates glucose, glycerol or formate [13]. Nitrate reductase activities of permeabilized bacteria incubated with 1 mM nitrate and reduced Methyl Viologen were determined as described previously [16].

### SDS/PAGE and chemical assays

SDS/PAGE was performed exactly as described by Tanapongpipat et al. [23]. Aerobic and anaerobic cultures were grown and assayed for $\beta$-galactosidase activity as described previously [23]. Nitrite concentrations were measured according to Pope and Cole [22]. Protein concentrations were determined by the Folin method.

## RESULTS

### Requirement for both NapG and NapH for rapid electron transfer from ubiquinol to the Nap

We have demonstrated previously that a strain lacking both NapG and NapH is defective in electron transfer from ubiquinol to the periplasmic NapCBA complex [16]. Two additional strains, JCB4146 deleted for only *napG* and JCB4147 defective only for NapH, were constructed to determine whether both NapG and NapH are essential for electron transfer from ubiquinol to NapC. These mutants, the original *ΔnapGH* deletion strain JCB4143 and the *nap*$^+$ parental strain JCB4141 were grown anaerobically in minimal medium supplemented with glycerol and 20 mM nitrate (Figure 1). In contrast with the parental strain, which grew with a specific growth rate of 0.21 h$^{-1}$, no significant growth of any of the mutants was detected, confirming that NapG and NapH are both required for rapid electron transfer from ubiquinol via NapC to the NapB–NapA complex. Anaerobic, Nap-dependent growth of all of the mutants was restored by transformation with the *napGH* plasmid pAN302N.

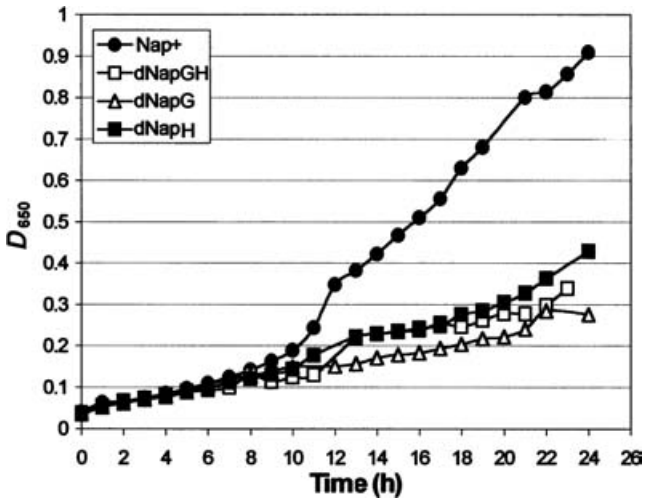


**Figure 1 Essential roles for both NapG and NapH in nitrate-dependent growth of strains defective in naphthoquinone synthesis**

Strains defective in naphthoquinone synthesis and expressing only the Nap were grown anaerobically in minimal medium with glycerol as the non-fermentable carbon source, and 20 mM nitrate as the only terminal electron acceptor. All four strains are defective in menaquinone synthesis (Men$^-$), so electrons are transferred from physiological substrates to nitrate via the ubiquinone pool (Ubi$^+$). ●, Strain JCB4141 (Nap$^+$Ubi$^+$ Men$^-$); □, strain JCB4143 (Ubi$^+$ Men$^-$ but Δ*napGH*); △, strain JCB4146 (Ubi$^+$ Men$^-$ but Δ*napG*); ■, strain JCB4147 (Ubi$^+$ Men$^-$ but Δ*napH*).

To determine the effects of single deletions of either *napG* or *napH* on rates of nitrate reduction by physiological substrates, the mutants and isogenic parental strains were grown in minimal medium containing 20 mM nitrate. As strains expressing only ubiquinone cannot grow anaerobically with glycerol as the carbon source, glucose was used despite its repressive effect on *nap* gene expression. Rates of nitrate reduction by formate measured with the nitrate electrode were almost below the limits of detection, at most 2 ($\pm$ 1) nmol · min$^{-1}$ · (mg of dry mass)$^{-1}$, compared with a rate of 18 nmol · min$^{-1}$ · (mg of dry mass)$^{-1}$ for the parental strain. The corresponding nitrate reduction rates with glucose as the electron donor were 18 ($\pm$ 0.5) nmol · min$^{-1}$ · (mg of dry mass)$^{-1}$ for the *nap*$^+$ parental strain and 4 ($\pm$ 2) nmol · min$^{-1}$ · (mg of dry mass)$^{-1}$ for the various mutants. Nitrate reductase activities measured with methyl viologen as the electron donor were similar for all strains, i.e. 25–50 nmol · min$^{-1}$ · (mg of dry mass)$^{-1}$, although variations between experiments were much greater in this assay, especially for the *napG* deletion mutant. These results established that expression of *napA* is similar in all of these strains, and were consistent with the view that NapG and NapH function together to facilitate electron transfer from ubiquinol via NapC to the NapAB complex.

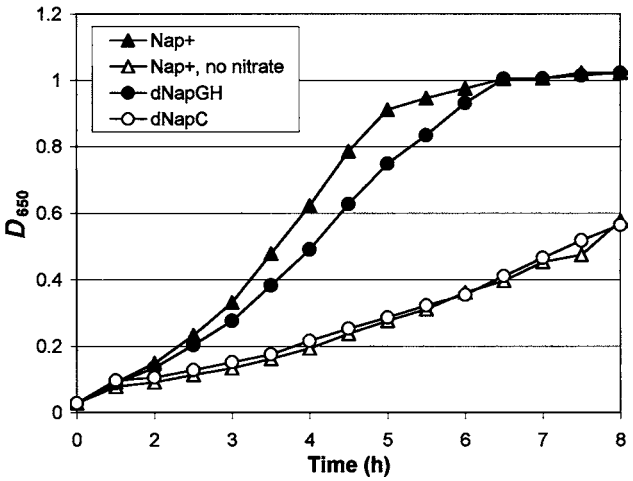


**Figure 2 Nitrate-stimulated growth of a strain defective in NapG and NapH during anaerobic growth with glucose as the fermentable carbon source**

Bacteria were grown in minimal medium supplemented with 5 % (v/v) LB with glucose as the fermentable carbon source. ▲, The Nap$^+$ strain JCB4141 in the presence of both glucose and 20 mM nitrate; △, strain JCB4141 in the absence of nitrate; ●, strain JCB4143 (Ubi$^+$ Men$^-$ but Δ*napGH*) in the presence of nitrate; ○, strain JCB4145 in the presence of nitrate. Note that despite the very low rate of nitrate reduction by strain JCB4143, this strain still responds to nitrate during glucose fermentation. All four strains are defective in naphthoquinone synthesis.

### A possible redox-balancing role for Nap

In the absence of menaquinone and membrane-associated nitrate reductase activity, anaerobic growth on glycerol/nitrate medium is dependent on the presence of both NapG and NapH. As the rate of nitrate reduction by a Δ*napGH* Δ*menBC* strain (JCB4143) was too low to be detected using a nitrate electrode, we concluded that NapG and NapH are essential for ubiquinol oxidation by Nap [16]. However, *E. coli* uses fumarate reductase for redox balancing during glucose fermentation, and fumarate reductase is a menaquinone-dependent enzyme [24,25]. In the absence of menaquinone, redox balancing must therefore be achieved by an alternative mechanism. Growth of the menaquinone-deficient, Nap$^+$ NarA$^-$ strain JCB4141 on glucose was far more rapid in the presence of nitrate than in its absence (Figure 2). The role of Nap in this case is not respiration, because there was no difference in the growth rate on glucose of the Ubi$^+$ Men$^+$ strain JCB4041, in the presence or absence of nitrate (results not shown). Furthermore, the Δ*napC*, Δ*menBC* mutant JCB4145, which is totally devoid of residual Nap activity, grew very slowly in the presence of glucose, but this rate was not increased in the presence of nitrate. In the absence of nitrate, the growth rate of the Δ*napGH* strain JCB4143 was identical with that of the *napC* deletion mutant (results not shown), but was almost the same as that of strain JCB4141 in the presence of nitrate (Figure 2). These results indicate that there is a residual Nap activity even in the Δ*napGH* Δ*menBC* strain JCB4143, which is dependent on ubiquinone and NapC. Although this residual activity is too low to be measured reliably with a nitrate electrode or to sustain normal growth in a glycerol/nitrate medium, it is apparently sufficient to replace fumarate reduction in its redox-balancing role during glucose fermentation.

The only additional evidence for a residual nitrate reductase activity in strain JCB4143 was the accumulation of traces of nitrite during growth in the presence of glucose and nitrate. In contrast, no nitrite was detected in cultures of the *napC* mutant JCB4145. To determine this residual rate more accurately, a set of mutants defective in the nitrite reductases Nir and Nrf was constructed so that nitrate reduction rates in the Δ*napGH*, Δ*menBC* background could be measured by determining the rate of nitrite accumulation. Growth rates and yields of strains JCB4181 (Nap$^+$, Δ*menBC*, Δ*nrfAB*, Δ*nirBCD*::kan) and JCB4183 (Δ*napGH*, Δ*menBC*, Δ*nrfAB*, Δ*nirBCD*::kan) were similar to each other and to the strains shown in Figure 2, but nitrite production was more than 10-fold lower in the NapGH deletion strain (0.1 mM compared with 1.4 mM nitrite in the growth medium). Therefore the residual nitrate reductase activity with ubiquinol as the electron donor in the absence of NapGH is at least 10-fold lower than the activity in the presence of NapGH. This residual rate, which was calculated to be in the range 1–2 nmol · min$^{-1}$ · (mg of dry mass)$^{-1}$, was consistent with the previous estimate based on nitrate electrode experiments.

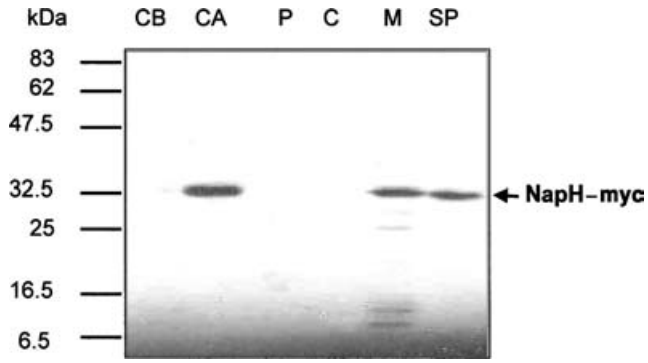


**Figure 3 Localization of NapH in *E. coli* membranes detected by Western-blot analysis**

*E. coli* TOP10 was transformed with the pBAD plasmid, pAN302N, encoding untagged NapG and NapH–myc–His$_6$, cloned into the Invitrogen vector pBAD/myc-His. Transformed bacteria were grown aerobically in 1 litre of LB and, when in the mid-exponential phase of growth, induced with 0.02 % L-arabinose for 4 h. Bacteria were harvested, washed and fractionated. After separation of 300 μg of protein by SDS/PAGE, proteins were transferred to a PDVF membrane and probed with anti-myc antibodies. Cross-reactive bands were detected by enhanced chemiluminescence. CB, cells before induction; CA, cells after induction for 4 h with 0.02 % arabinose; P, C and M, the periplasmic, cytoplasmic and membrane-associated fractions respectively; SP, slow-spin pellet containing unbroken bacteria and inclusion bodies.

### Localization of NapH determined by Western-blotting experiments

On the basis of its primary structure, NapH is predicted to be an integral membrane protein, but so far this has not been confirmed experimentally. To determine its localization, NapH was expressed with a C-terminal fusion to a myc/His$_6$ tag. NapG and NapH were expressed together because there are indications that these proteins are unstable when expressed individually. After cellular fragmentation, the membrane fraction was further purified on a sucrose gradient to exclude any contamination with other fractions. A cross-reacting band of approx. 32 kDa was detectable in the membrane fraction and in the low-spin fraction sedimented by slow-speed centrifugation, which contained unbroken cells and possible inclusion bodies (Figure 3). The apparent molecular mass of this band corresponds to that expected for NapH–myc–His$_6$. No cross-reacting band was detected in either the cytoplasmic or the periplasmic fractions. Therefore, it was confirmed that NapH is indeed localized in the membrane.

### Topology of NapH deduced from alkaline phosphatase and β-galactosidase fusions

On the basis of the hydropathy profile, there are two possible models for the folding of NapH through the membrane (Figures 4a and 4b). The hydropathy profile shows four highly hydrophobic

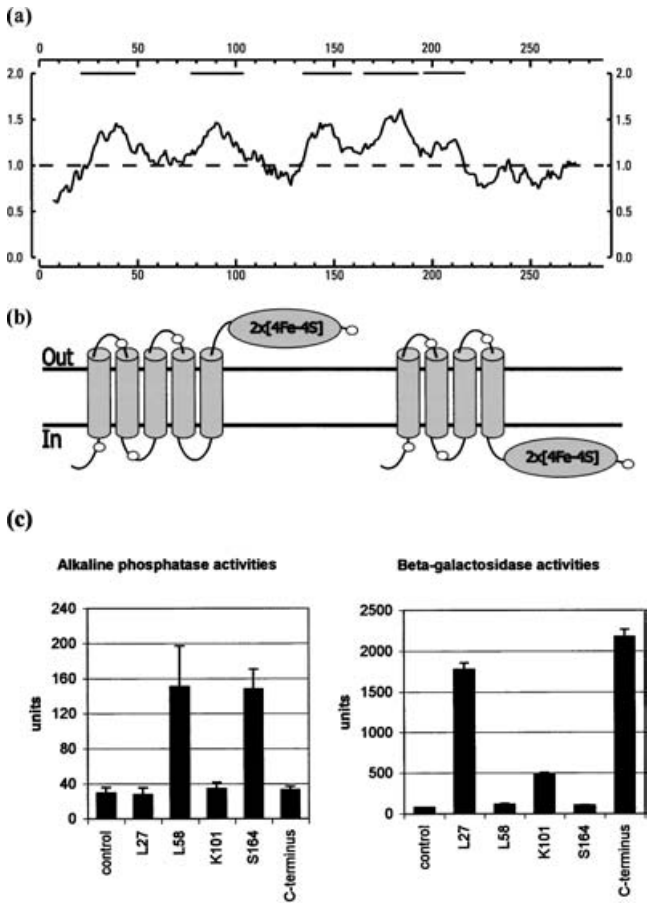


**Figure 4 Topology of NapH predicted from hydrophobicity plots and deduced from alkaline phosphatase and $\beta$-galactosidase fusion results**

(**a**) Hydropathy plot of NapH. (**b**) Alternative predicted folding of NapH into the cytoplasmic membrane based on different topology prediction programmes. Open circles indicate the fusion junctions with PhoA and LacZ. (**c**) Alkaline phosphatase and $\beta$-galactosidase activities of bacteria transformed with plasmids carrying in-frame fusions of different N-terminal fragments of NapH with PhoA and LacZ. Units are nmol of X-Gal or X-P hydrolysed $\cdot$ min$^{-1}$ $\cdot$ (mg of bacterial dry mass)$^{-1}$.

stretches that are predicted to be membrane-spanning helices. However, there is a fifth hydrophobic region that is less hydrophobic than the other four. Depending on the prediction method used, this fifth hydrophobic region either is predicted to be a membrane-spanning helix or is included within the soluble C-terminal domain. To discriminate between the alternative models and to determine the positions of the N- and C-termini relative to the cytoplasmic membrane, a series of alkaline phosphatase (PhoA) and $\beta$-galactosidase (LacZ) fusion proteins was constructed.

Compared with the control strain without a fusion protein, high LacZ and low PhoA activities were associated with fusion proteins having 27 N-terminal residues of NapH (Figure 4c). The N-terminus of NapH is therefore localized in the cytoplasm. The fusions at positions 58 and 164 were predicted to be located in the periplasm by both models. This was confirmed by the high PhoA and low LacZ activities observed for these fusions. Similarly, the fusions at position 101 were predicted to be in the cytoplasm and this was also confirmed. The two alternative models predict opposite locations for the C-terminal domain. Fusions to the C-terminal domain gave high LacZ activity and low PhoA activity. Therefore, the C-terminal domain of NapH

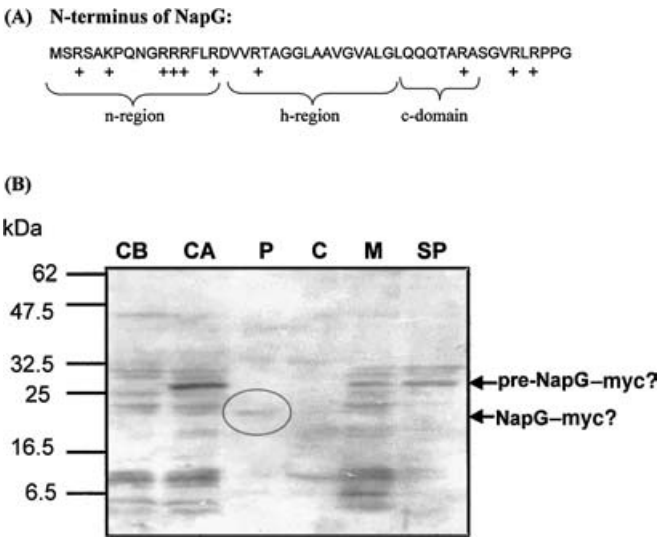


**Figure 5 N-terminal amino acid sequence and subcellular location of NapG**

(**A**) N-terminal amino acid sequence of NapG, showing the positively charged n-region together with the twin-arginine motif, the hydrophobic h-region and the c-domain including a possible signal peptide cleavage site. (**B**) Attempts to detect apo-NapG and NapG in the membrane and periplasmic fractions by Western-blot analysis. *E. coli* TOP10 was transformed with the pBAD derivative plasmid, pAN303, encoding both NapG with an N-terminal myc tag and napH. Bacteria were grown in 2 litres of anaerobic minimal medium supplemented with glycerol/nitrite. CB, CA, cells respectively before and after induction with 0.02 % L-arabinose; P, M and C, periplasmic, membrane-associated and cytoplasmic proteins respectively from cells harvested after induction. SP, the slow-speed pellet containing unbroken bacteria and inclusion bodies.

is located in the cytoplasm, indicating that NapH inserts into the membrane with four membrane-spanning domains.

## TAT of NapG to the periplasm

NapG and NapH are usually found together in the *nap* operons of different bacteria, indicating that they might be co-translated and function as a complex. The C-terminal, cytoplasmic domain of NapH contains two putative 4Fe–4S clusters. NapG is predicted to be a soluble non-haem iron–sulphur protein with four 4Fe–4S clusters. If the assumption is made that the iron–sulphur clusters of NapG and NapH are involved in electron transfer from ubiquinol to NapA, one might expect NapG to be in close contact with the C-terminal domain of NapH. Since the C-terminal domain of NapH is located in the cytoplasm, this would then also be the expected position of NapG. Preliminary experiments in which *napG* was fused in-frame at the codon for Ala-60 and at the C-terminal Ser-231 to both *phoA* in plasmid pSK4158 and *lacZY* in pNM480 seemed to confirm this expectation. The four resulting plasmids were transformed into *E. coli* TOP10 and purified transformants were plated on to both X-Gal and X-P plates. Bacteria transformed with the NapG–LacZ fusions formed blue colonies on X-Gal plates; those transformed with NapG–PhoA plasmids formed white colonies on X-P plates. When assayed quantitatively, no significant alkaline phosphatase activity was detected, but 1400 and 1800 units of $\beta$-galactosidase activity were detected for the Ala-60 and Ser-231 fusions, respectively.

Although the above results suggested that NapG is a soluble, cytoplasmic protein, the N-terminus of NapG is reminiscent of a TAT-dependent export signal (Figure 5A) that includes a clearly recognizable, positively charged n-region followed by a hydrophobic h-region. Also, a putative leader peptidase cleavage site between positions 41 and 42 is clearly recognizable. Furthermore,

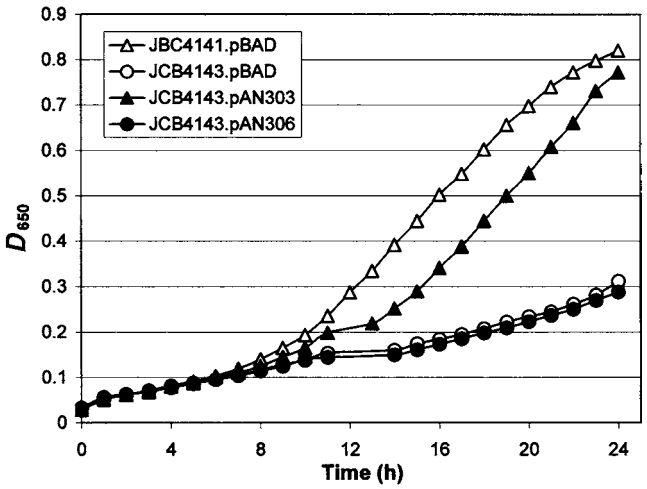


**Figure 6 Requirement for the twin-arginine motif for complementation of a *napG* deletion by *napG*$^+$ on a multi-copy plasmid**

Bacteria were grown anaerobically in a minimal medium supplemented with the non-fermentable carbon source, glycerol, and 20 mM nitrate. Strain JCB4143 is a *ΔnapGH* derivative of the Nap$^+$ Ubi$^+$ Men$^-$ strain, JCB4141. Plasmid AN303 encodes functional *naPG* and *naPH* genes; plasmid AN306 (derived from AN303) encodes a modified NapG with RA substitutions at positions 11 and 12 in the putative twin-arginine targeting motif.

NapG contains a GRRRFLR sequence in the n-region, which is similar to the (S/T)RRxFLK consensus recognition signal for the TAT system [14,15,26,27]. On the basis of its primary structure, NapG is therefore predicted to be transported to the periplasm via the TAT secretion pathway. It is well established that LacZ and PhoA fusions of TAT-dependent target proteins yield results contrary to expectation [28].

To confirm the cellular location of NapG, a plasmid was constructed for the overexpression of NapG–myc, similar to that used for the localization of NapH. After cellular fractionation, a cross-reacting band of approx. 27 kDa was clearly visible in the membrane and slow spin fractions (Figure 5B). This band corresponds in size to that expected for unprocessed NapG–myc. However, a cross-reacting band of about 22 kDa was detected in the periplasmic fraction (Figure 5B). This band corresponds in size to that expected for NapG–myc when cleaved at the predicted leader peptidase cleavage site. We therefore propose that the band detected in the membrane fraction is uncleaved pre-NapG–myc that accumulates due to the overexpression of NapG, whereas the band detected in the periplasm is the processed NapG–myc at its correct location. Note, however, that in contrast with Western-blot experiments with the same antibody and detection system used for the analysis of the cellular localization of NapH, many additional cross-reacting bands were always detected in these experiments. Attempts to avoid these additional bands, or to provide more convincing evidence for the periplasmic location of NapG, were unsuccessful.

To confirm the location of NapG and the importance of the twin-arginine signal in targeting it to the periplasm, a mutated derivative of *napG* in plasmid pAN306 (encoding NapG lacking its twin-arginine signal) was compared with plasmid pAN303 for its ability to complement a NapGH deletion strain (Figure 6). A *ΔnapGH, ΔmenBC* strain (JCB4143) could not grow anaerobically in glycerol/nitrate medium [16]. However, growth was substantially restored if NapG and NapH were expressed from plasmid pAN303. Plasmid pAN306 was constructed such that the twin-arginine motif was substituted by alanine residues. This plasmid was unable to complement the growth defect of strain JCB4143 (Figure 6). Therefore the twin-arginine sequence is essential for NapG function, presumably because it is needed for correct targeting of NapG to the periplasm.

**Table 3 Two-hybrid interactions between NapC, NapG and NapH**

+, A positive interaction as shown on MacConkey-lactose plates; −, no interaction; nd, not determined. The number of + symbols indicates the strength of the interaction. The time required for red colonies to develop is given inparentheses.

| | | Interaction | | |
|---|---|---|---|---|
| Protein | Plasmid | T25–NapC pKT25-C | T25–NapG pKT25-G | T25–NapH pKT25-H |
| NapC–T18 | pUT18-C | − | − | − |
| T18–NapC | pUT18C-C | +++ (18 h) | − | ++ (24 h) |
| NapG–T18 | pUT18-G | − | − | − |
| T18–NapG | pUT18C-G | − | − | − |
| NapH–T18 | pUT18-H | − | − | + (36 h) |
| T18–NapH | pUT18C-H | + (36 h) | − | − |

### Use of a bacterial two-hybrid assay to detect interactions between NapC, NapG and NapH

A bacterial two-hybrid system has been developed to detect interactions between two proteins either in the cytoplasm or on the cytoplasmic side of the cytoplasmic membrane [21,29,30]. This system is based on interaction-mediated restoration of adenylate cyclase activity. Two proteins of interest are expressed as fusion proteins with two fragments, T25 and T18, of *B. pertussis* adenylate cyclase. If the two proteins interact, a functional adenylate cyclase is formed and therefore cAMP is produced. The adenylate cyclase activity can be monitored by following the ability of an *E. coli cya* mutant to utilize maltose or lactose or by measuring the resulting $\beta$-galactosidase activity. The possibility that NapC, NapG and NapH interact within the bacterial membrane was investigated.

All possible combinations of NapC, NapG and NapH were checked for their ability to interact (Table 3). A strong interaction was shown between NapC and NapH, provided that the NapC tag was located on the N-terminus, which is consistent with the predicted localization of the C-terminus of NapC in the periplasm. This strong interaction between NapC and NapH is consistent with NapC and NapH forming part of the same electron transport chain. There are strong indications that NapC, and possibly also NapH, forms a multimeric complex. However, any interaction between two tagged NapH proteins was fairly weak. No evidence for interactions of NapG with any component was obtained. As this assay was designed to detect protein–protein interactions in the cytoplasm, this negative result is consistent with the proposed periplasmic location of NapG.

### Use of menadiol as an exogenous quinol to confirm the physiological role of NapG and NapH

The results presented above and previously [16] indicate that the physiological role of NapG and NapH is to facilitate electron transfer from $UQH_2$ (reduced ubiquinone), but not from $MKH_2$ (reduced menaquinone), to NapC. The midpoint redox potential for the menaquinone:$MKH_2$ couple is lower than that of the ubiquinone:$UQH_2$ couple (−70 mV compared with +90 mV), suggesting that NapG and NapH might be required to couple the oxidation of the weaker electron donor to NapC reduction. Artificial ubiquinone and menaquinone analogues were tested for their ability to support NapGH-dependent electron transfer via NapC to the NapAB complex. Preliminary experiments

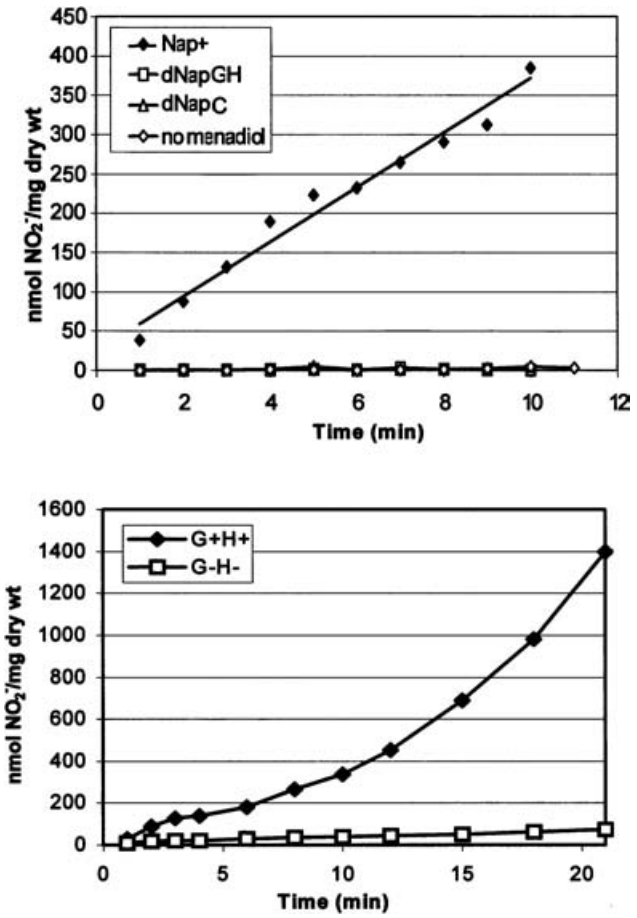


**Figure 7** ***In vitro*** **reduction of nitrate to nitrite using reduced menadiol as the electron donor**

A stock solution of 5 mM menadione was reduced with sodium borohydride immediately before use. Suspensions of washed bacteria were stirred with 5 mM nitrate and 1 mM electron donor at room temperature, and the quantity of nitrite accumulated by samples withdrawn at regular intervals was determined. Upper panel: strains used were defective in menaquinol synthesis. ◆, Strain JCB4141 (Nap$^+$ Ubi$^+$ Men$^-$); □, strain JCB4143 (Ubi$^+$ Men$^-$ Δ*napGH*); △, Ubi$^+$ Men$^-$ Δ*napC*; ◇, negative control, strain JCB4141 without added menadiol. Lower panel: strains used for these experiments were JCB4081 and JCB4083 that lacked both nitrite reductases, Nir and Nrf, but were competent for both ubiquinol and menaquinol synthesis. ◆, Strain JCB4081 (Nap$^+$ Ubi$^+$ Men$^+$ Nir$^-$ Nrf$^-$); □, strain JCB4083 (Nap$^+$ Ubi$^+$ Men$^+$ Nir$^-$ Nrf$^-$ Δ*napGH*). Dry wt, dry mass.

established that the water-soluble $UQ_0$ (ubiquinone analogue with no isoprenyl side chains) and plumbagin are poor electron donors to the Nap, and the low-midpoint-potential analogue lapachol gave poorly reproducible rates. High rates of nitrate reduction were detected using menadiol as the exogenous electron donor for resting cell suspensions of strain JCB4141, but not for strain JCB4143, and this rate was totally dependent on the presence of NapC, as shown by the inability of strain JCB4145 to catalyse nitrate reduction by menadiol (Figure 7, upper panel). Similar results were obtained with strains JCB4041 and 4043, which synthesize both $MKH_2$ and $UQH_2$. As all of the above strains were Nir$^+$ and Nrf$^+$ and therefore potentially able to reduce nitrite formed during nitrate reduction, Nir$^-$ Nrf$^-$ derivatives of strains JCB4041 and 4043 were constructed. The rate of nitrate reduction by the NapG$^+$ NapH$^+$ strain JCB4081 in the presence of menadiol was 100 ($\pm$27) nmol of nitrite formed $\cdot$ min$^{-1}$ $\cdot$ (mg of bacterial dry mass)$^{-1}$ compared with a rate of 3 ($\pm$2) nmol of nitrite formed $\cdot$ min$^{-1}$ $\cdot$ (mg of bacterial dry mass)$^{-1}$ for the NapG NapH-

**Table 4 Rates of nitrite production with artificial electron donors [nmol of $NO_2^-$ $\cdot$ min$^-$ $\cdot$ (mg of dry mass$^{-1}$)] in NapGH$^+$ and ΔNapGH strains**

MeV, Methyl Viologen.

| Strain | Nitrite production | | Relative activity (MeV/menadiol) |
|---|---|---|---|
| | Menadiol | MeV | |
| JCB4081 (Nap$^+$) | 100 $\pm$ 27 | 205 $\pm$ 108 | 2.05 |
| JCB4083 (Δ*napGH*) | 3 $\pm$ 2 | 42 $\pm$ 11 | 14.0 |

defective strain, JCB4083 (Figure 7, lower panel). As these strains were competent for both menaquinol and ubiquinol synthesis, it can be concluded that menadiol transfers electrons only into the ubiquinol branch of the electron-transfer pathway to NapC, and that NapG and NapH are required for normal rates of electron transfer from ubiquinol to NapC. Although the Methyl Viologen-dependent rate of nitrate reduction was also lower for strain JCB4083 than for strain JCB4081, the difference was insufficient to account for the dependence of nitrate reduction by menadiol on NapG and NapH (Table 4).

## DISCUSSION

We previously proposed that NapG and NapH are not involved in menaquinol oxidation, but function as energy-conserving quinol dehydrogenase during electron transfer from ubiquinol via NapC and NapB to NapA [16]. This proposal was based on the observation that deletion of the *napF* gene from the parental strain resulted in severely decreased growth rate and yield, a phenotype that was reversed by the additional deletion of both *napG* and *napH* [16]. The results were consistent with the function of NapF being capable of maintaining the correct directionality of proton translocation by the energy-conserving quinol dehydrogenase, NapH. Such a role implies that the yield of biomass of a *napGH* mutant during anaerobic, nitrate-limited growth should be lower than that of an isogenic parental strain. We have now shown that this is incorrect (Figure 1).

The growth rate of the Ubi$^+$ Men$^-$ Nap$^+$ strain JCB4141 in the presence of the fermentable carbon source glucose was greatly stimulated by addition of nitrate, but the final yield of biomass was unaffected. This increased growth rate was Nap-dependent, as shown by the lack of nitrate stimulation in the *napC* mutant, strain JCB4145 (Figure 2). These results strongly suggest that Nap fulfils a redox-balancing role rather than an energy-conservation role during anaerobic growth by glucose fermentation. Despite the very low rates of nitrate reduction by the *napGH* mutant, strain JCB4143, nitrate still stimulated growth to a rate only slightly lower than for the Nap$^+$ parental strain. This growth stimulation was totally reproducible between experiments and was not due to reversion or unmasking of an additional nitrate reductase activity. Bacteria harvested at the end of these growth experiments reduced nitrate at a rate that was at most 1 % of that of the parental strain JCB4141. This revealed that, during glucose fermentation, very low rates of nitrate respiration have profound effects on growth kinetics.

On the basis of our localization studies, the iron–sulphur clusters of NapG and NapH are located on opposite sides of the membrane. However, since the cytoplasmic domain of NapH contains a fairly hydrophobic stretch of amino acids, it is possible that this domain is partially inserted into the membrane. NapG also has a rather hydrophobic patch and might therefore also partially insert into the periplasmic side of the membrane. If

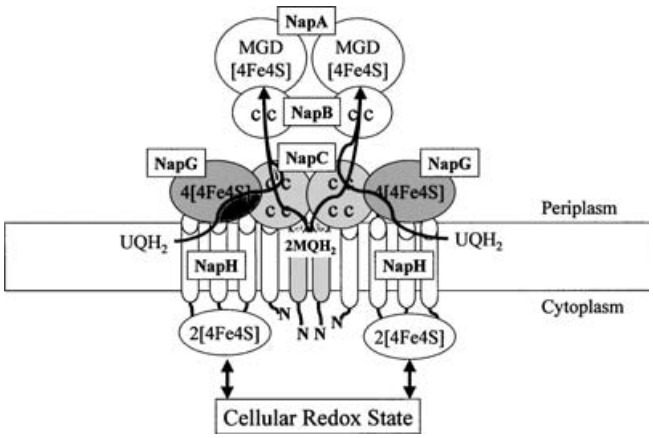


**Figure 8 Working model for electron transfer from the cytoplasm via ubiquinone, NapH and NapG to the NapCBA complex in the periplasm**

MGD, molybdopterin guanine dinucleotide.

NapG binds to NapH, it is possible that the iron–sulphur clusters of the two proteins are in sufficiently close proximity to allow electron transfer between them. We previously used a *ΔnapGH* double mutant to conclude that one or both of NapG and NapH are essential for nitrate reduction using ubiquinol as the electron donor. This would be consistent with the proposed roles of NapG and NapH in *Wolinella succinogenes*, a bacterium that lacks both the NapC homologue and ubiquinone [32]. We assume that, in *Wolinella*, NapGH is the only functional quinol dehydrogenase that transfers electrons to NapB and NapA, but in this case the electron donor is the lower-potential menaquinol rather than ubiquinol. Single deletions of either *napG* or *napH* in the $Men^-$ $Ubi^+$ and $Men^+$ $Ubi^+$ backgrounds have now been used to demonstrate that, in *E. coli*, both NapG and NapH are required for rapid electron transfer from ubiquinol via NapC to NapB and NapA. We therefore conclude that NapG and NapH are part of the same electron-transfer pathway from ubiquinol to NapC and ultimately to NapA.

Menadiol was an effective electron donor to Nap *in vitro*, but only in the complete Nap system of strains JCB4041, JCB4081 and JCB4141 (Figure 7, Table 4 and results not shown). In the absence of NapG and NapH (strains 4043, 4083 and 4143) there was only a minimal rate of nitrate reduction by menadiol. This confirms the role of NapG and NapH in the oxidation of some, but not all, quinols. Although menadiol appears to be a closer structural analogue of menaquinol than ubiquinol [25], its midpoint redox potential is closer to that of the ubiquinone–ubiquinol couple. It has been shown before that quinol analogues can behave unexpectedly based on their structural similarity to the natural quinols. Armstrong and co-workers [33] have demonstrated that alterations in driving force (midpoint redox potential) can alter respiratory enzyme rates, an indication that biology tunes rates to match the availability of reducing equivalents. The midpoint potentials of quinol analogues may be very far from those of their structural analogues and this may play a major role in determining their ability to donate electrons. Therefore, in our *in vitro* system, menadiol seems to behave more like a ubiquinol analogue rather than as a menaquinol analogue.

Figure 8 summarizes current knowledge of the roles of NapG and NapH in the transfer of electrons from ubiquinol via NapC and NapB to NapA. The alternative route from menaquinol to NapC, which is independent of NapG and NapH, is also shown. There must also be a third, minor electron-transfer pathway from ubiquinol directly to NapC, but as this accounts for less than 1 % of the total rate of nitrate reduction, it has been omitted from the Figure. Nevertheless, this low rate is sufficient to fulfil the redox-balancing requirements during glucose fermentation in the absence of a functional fumarate reductase. This working model accounts not only for earlier work [16], but also for the cellular location of NapH, as determined by Western-blot analysis using anti-Myc antibody (Figure 3), and the topological analysis using PhoA and LacZ fusions (Figure 4). As the iron–sulphur centres of NapH are on the cytoplasmic side of the membrane, they are unlikely to be involved directly in electron transfer: could their function be to monitor the redox state of the cytoplasm? If so, any conformational change resulting from oxidation or reduction of the iron–sulphur centres might modulate the flux through the two quinone pools. The two-hybrid results suggest that NapC interacts with itself, forming a dimer (as indicated in the Figure) or a higher multimer. NapH also interacts strongly with NapC, but only weakly with itself (Table 3). The effects of mutagenesis of the twin-arginine motif at residues 11 and 12 of NapG, together with weaker evidence from Western blotting and the negative data from two-hybrid experiments, all indicate that NapG is located in the periplasm. However, both NapG and NapH are individually essential for effective electron flow from ubiquinol to NapC. Hence it is proposed that electrons are transferred sequentially from ubiquinol to NapH and then to NapG.

The demonstration that there are two, partially independent, electron-transfer pathways to the Nap raises the fascinating question as to why both have been retained. As a facultative anaerobe, *E. coli* must be capable of adapting to aerobic and anaerobic environments. NapGH appears to be important during the transition to anoxia, sustaining $UQH_2$-dependent nitrate reduction during increased synthesis of the $MKH_2$ pool. *E. coli* most commonly live under conditions of limited oxygen supply, but also with limited supplies of alternative electron acceptors such as nitrate in their environment. Under such conditions, the higher-midpoint-potential ubiquinone–ubiquinol couple will be partially reduced, but the lower midpoint potential menaquinone–menaquinol couple will be essentially oxidized. Under these conditions, a low rate of nitrate respiration provided by the NapG–NapH pathway might be sufficient to maintain redox-balanced growth. In contrast, in the absence of oxygen, both quinone pools will be reduced, and hence the more rapid menaquinol pathway will ensure rapid electron transfer not only to Nap, but also to the formate-dependent nitrite reductase, Nrf. This pathway will consume eight electrons, making available four molecules of $NAD^+$ for fermentative growth. For the first time, direct experimental evidence to prove that the *E. coli* Nap can fulfil the redox-balancing role implied by the above model has been demonstrated (Figure 2).

We are grateful to Lesley Griffiths for expert technical assistance, to Daniel Ladant for making available plasmids for the bacterial two-hybrid experiments and to the UK Biotechnology and Biological Sciences Research Council for financial support. A. N. was funded by a Training Scholarship from the Royal Thai Government.

## REFERENCES

1 Berks, B. C., Ferguson, S. J., Moir, J. W. and Richardson, D. J. (1995) Enzymes and associated electron transport systems that catalyse the respiratory reduction of nitrogen oxides and oxyanions. Biochim. Biophys. Acta **1232**, 97–173

2 Blasco, F., Iobbi, C., Ratouchniak, J., Bonnefoy, V. and Chippaux, M. (1990) Nitrate reductases of *Escherichia coli*: sequence of the second nitrate reductase and comparison with that encoded by the *narGHJI* operon. Mol. Gen. Genet. **222**, 104–111

3 Iobbi-Nivol, C., Santini, C. L., Blasco, F. and Giordano, G. (1990) Purification and further characterization of the second nitrate reductase of *Escherichia coli* K12. Eur. J. Biochem. **188**, 679–687

4 Stewart, V. (1988) Nitrate respiration in relation to facultative metabolism in enterobacteria. Microbiol. Rev. **52**, 190–232

5 Potter, L. C., Millington, P., Griffiths, L., Thomas, G. H. and Cole, J. A. (1999) Competition between *Escherichia coli* strains expressing either a periplasmic or a membrane-bound nitrate reductase: does Nap confer a selective advantage during nitrate-limited growth? Biochem. J. **344**, 77–84

6 Iobbi, C., Santini, C. L., Bonnefoy, V. and Giordano, G. (1987) Biochemical and immunological evidence for a second nitrate reductase in *Escherichia coli* K12. Eur. J. Biochem. **68**, 451–459

7 Richardson, D. J. and Ferguson, S. J. (1992) The influence of carbon substrate on the activity of the periplasmic nitrate reductase in aerobically grown *Thiosphaera pantotropha*. Arch. Microbiol. **157**, 535–537

8 Reyes, F., Roldan, M. D., Klipp, W., Castillo, F. and Moreno-Vivian, C. (1996) Isolation of periplasmic nitrate reductase genes from *Rhodobacter sphaeroides* DSM 158: structural and functional differences among prokaryotic nitrate reductases. Mol. Microbiol. **19**, 1307–1318

9 Reyes, F., Gavira, M., Castillo, F. and Moreno-Vivian, C. (1998) Periplasmic nitrate-reducing system of the phototrophic bacterium *Rhodobacter sphaeroides* DSM 158: transcriptional and mutational analysis of the *napKEFDABC* gene cluster. Biochem. J. **331**, 897–904

10 Sears, H. J., Sawers, G., Berks, B. C., Ferguson, S. J. and Richardson, D. J. (2000) Control of periplasmic nitrate reductase gene expression (*napEDABC*) from *Paracoccus pantotrophus* in response to oxygen and carbon substrates. Microbiology **146**, 2977–2985

11 Potter, L., Angove, H., Richardson, D. and Cole, J. (2001) Nitrate reduction in the periplasm of Gram-negative bacteria. Adv. Microb. Physiol. **45**, 51–112

12 Berks, B. C., Richardson, D. J., Reilly, A., Willis, A. C. and Ferguson, S. J. (1995b) The *napEDABC* gene cluster encoding the periplasmic nitrate reductase system of *Thiosphaera pantotropha*. Biochem. J. **309**, 983–992

13 Potter, L. C. and Cole, J. A. (1999) Essential roles for the products of the napABCD genes, but not napFGH, in periplasmic nitrate reduction by *Escherichia coli* K-12. Biochem. J. **344**, 69–76

14 Berks, B. C., Sargent, F. and Palmer, T. (2000) The Tat protein export pathway. Mol. Microbiol. **35**, 260–274

15 Weiner, J. H., Bilous, P. T., Shaw, G. M., Lubitz, S. P., Frost, L., Thomas, G. H., Cole, J. A. and Turner, R. J. (1998) A novel and ubiquitous system for membrane targeting and secretion of cofactor-containing proteins. Cell (Cambridge, Mass.) **93**, 93–101

16 Brondijk, T. H., Fiegen, D., Richardson, D. J. and Cole, J. A. (2002) Roles of NapF, NapG and NapH, subunits of the *Escherichia coli* periplasmic nitrate reductase, in ubiquinol oxidation. Mol. Microbiol. **44**, 245–255

17 Paulsen, I. T., Brown, M. H., Dunstan, S. J. and Skurray, R. A. (1995) Molecular characterization of the staphylococcal multidrug resistance export protein QacC. J. Bacteriol. **177**, 2827–2833

18 Minton, N. P. (1984) Improved plasmid vectors for the isolation of translational lac gene fusions. Gene **31** 269–273

19 Manoil, C. (1991) Analysis of membrane protein topology using alkaline phosphatase and $\beta$-galactosidase gene fusions. Methods Cell Biol. **34**, 61–75

20 Jayaraman, P.-S., Peakman, T. C., Busby, S. J. W., Quincey, R. V. and Cole, J. A. (1987) Location and sequence of the promoter of the gene for the NADH-dependent nitrite reductase of *Escherichia coli* and its regulation by oxygen, the Fnr protein and nitrite. J. Mol. Biol. **196**, 781–788

21 Karimova, G., Ullmann, A. and Ladant, D. (2000) A bacterial two-hybrid system that exploits a cAMP signaling cascade in *Escherichia coli*. Methods Enzymol. **328**, 59–73

22 Pope, N. R. and Cole, J. A. (1984) Pyruvate and ethanol as electron donors for nitrite reduction by *Escherichia coli* K12. J. Gen. Microbiol. **130**, 1279–1284

23 Tanapongpipat, S., Reid, E., Cole, J. A. and Crooke, H. (1998) Transcriptional control and essential roles of the *Escherichia coli ccm* gene products in formate-dependent nitrite reduction and cytochrome *c* synthesis. Biochem. J. **334**, 355–365

24 Kroger, A. (1978) Fumarate as terminal acceptor of phosphorylative electron transport. Biochim. Biophys. Acta **505**, 129–145

25 Soballe, B. and Poole, R. K. (1999) Microbial ubiquinones: multiple roles in respiration, gene regulation and oxidative stress management. Microbiology **145**, 1817–1830

26 Santini, C. L., Ize, B., Chanal, A., Muller, M., Giordano, G. and Wu, L. F. (1998) A novel sec-independent periplasmic protein translocation pathway in *Escherichia coli*. EMBO J. **17**, 101–112

27 Stanley, N. R., Palmer, T. and Berks, B. C. (2000) The twin arginine consensus motif of Tat signal peptides is involved in Sec-independent protein targeting in *Escherichia coli*. J. Biol. Chem. **275**, 11591–11596

28 Stanley, N. R., Sargent, F., Buchanan, G., Shi, J., Stewart, V., Palmer, T. and Berks, B. C. (1992) Behaviour of topological marker proteins targeted to the Tat protein transport pathway. Mol. Microbiol. **43**, 1005–1102

29 Karimova, G., Pidoux, J., Ullmann, A. and Ladant, D. (1998) A bacterial two-hybrid system based on a reconstituted signal transduction pathway. Proc. Natl. Acad. Sci. U.S.A. **95**, 5752–5756

30 Ladant, D. and Ullmann, A. (1999) *Bordetella pertussis* adenylate cyclase: a toxin with multiple talents. Trends Microbiol. **7**, 172–176

31 Stewart, V. and MacGregor, C. H. (1982) Nitrate reductase in *Escherichis coli* K-12: involvement of *chlC, chlE*, and *chlG* loci. J. Bacteriol. **151**, 788–799

32 Simon, J., Sänger, M., Schuster, S. C. and Gross, R. (2003) Electron transport to periplasmic nitrate reductase (NapA) of Wolinella succinogenes is independent of a NapC protein. Mol. Microbiol. **49**, 69–79

33 Elliott, S. J., Léger, C., Pershad, H. R., Hirst, J., Heffron, K., Ginet, N., Blasco, F., Rothery, R. A., Weiner, J. and Armstrong, F. A. (2002) Detection and interpretation of redox potential optima in the catalytic activity of enzymes. Biochim. Biophys. Acta **1555**, 54–59


Received 24 July 2003/1 December 2003; accepted 12 December 2003
Published as BJ Immediate Publication 16 December 2003, DOI 10.1042/BJ20031115